ACS Photonics

Article

pubs.acs.org/journal/apchd5

Probing Vertical and Horizontal Plasmonic Resonant States in the Photoluminescence of Gold Nanodisks

Liyong Jiang,[†,‡,#] Tingting Yin,[‡,#] Zhaogang Dong,[§] Hailong Hu,[∥] Mingyi Liao,[∥] David Allioux,[∥] Shawn J. Tan,[§] Xiao Ming Goh,[§] Xiangyin Li,[†] Joel K. W. Yang,[*,§,⊥] and Zexiang Shen[*,‡,∥]

[†]Nanophotonic Laboratory, Department of Physics, Nanjing University of Science and Technology, Nanjing 210094, China

[‡]Centre for Disruptive Photonic Technologies, School of Physical and Mathematical Sciences, Nanyang Technological University, 1 Nanyang Walk, Blk 5 Level 3, Singapore 637371, Singapore

[§]Institute of Materials Research and Engineering, A*STAR (Agency for Science, Technology and Research), 3 Research Link, Singapore 117602, Singapore

[∥]School of Physical and Mathematical Sciences, Nanyang Technological University, 21 Nanyang Link, Singapore 637371, Singapore

[⊥]Singapore University of Technology and Design, 8 Somapah Road, Singapore 487372, Singapore

Supporting Information

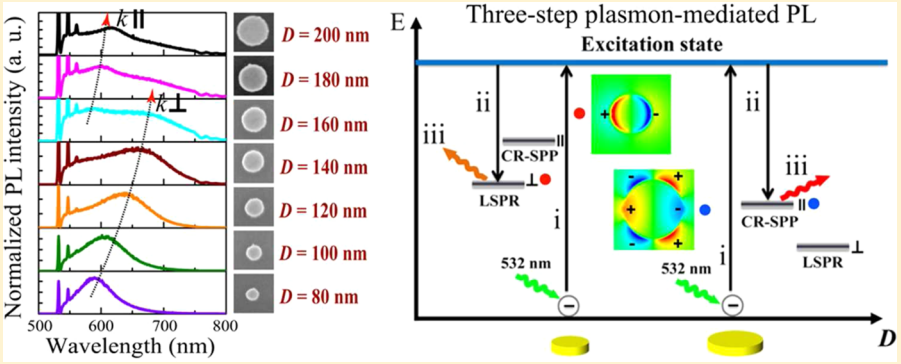

ABSTRACT: Localized surface plasmon resonance (LSPR) on gold nanoparticles and nanostructures shows its capability to modulate the spontaneous emission rate for photoluminescence. However, beyond the quasi-static limit with oblique incidence conditions, probing a retardation-based plasmonic resonant state excited by the horizontal incident wave-vector component has not been reported yet in the plasmon-mediated photoluminescence of gold nanostructures. In this paper, we investigated the photoluminescence of individual and coupled gold nanodisks with increasing size, and the peaks in the size-dependent photoluminescence spectra are shown to originate from the preferential excitation of vertical (LSPR) and horizontal (retardation-based) plasmonic resonant states. We have also proposed a three-step model to well describe the contribution of vertical and horizontal plasmonic resonant states in the photoluminescence of gold nanodisks. Our study makes a new contribution to the understanding of photoluminescence from gold nanostructures, and it paves the way toward the applications of plasmon-mediated luminescence and biological studies.

KEYWORDS: *gold nanodisks, retardation effects, localized surface plasmon resonance, photoluminescence, oblique incidence*

Due to the radiative recombination of holes in the d-band with electrons in the sp-band, visible photoluminescence (PL) has been demonstrated on gold films,[1] but its quantum yield is low ($\sim 10^{-10}$) due to the dominant nonradiative scattering of photoexcited carriers. Nonetheless, a much higher PL, with a quantum efficiency of $\sim 10^{-4}$, has been demonstrated on gold clusters, gold nanoparticles, and nanostructures.[2−11] In particular, significant enhancements of PL efficiency in nanoparticles and nanostructures with sizes larger than ∼20 nm are attributed to the localized surface plasmon resonance (LSPR), which acts as an additional ultrafast radiative channel in the femtosecond regime and thus enhances the radiative recombination of interband electrons and holes.[11]

Plasmon-mediated PL is now of great interest to scientists and has inspired a variety of attractive applications, such as plasmophore rulers,[12] mode mapping,[13−15] up-conversion luminescence,[16] protein detection,[17] and biological imaging and therapy.[18] However, some fundamental phenomena in plasmon-mediated PL still require further thorough investigations. For example, a consistent dynamic model is still missing to well describe the intrinsic relationship between the nonradiative relaxation of photoexcited carriers and the plasmonic resonant states in the PL process.[19−21] Moreover,

Received: June 2, 2015
Published: July 16, 2015

DOI: 10.1021/acsphotonics.5b00308
ACS Photonics 2015, 2, 1217−1223

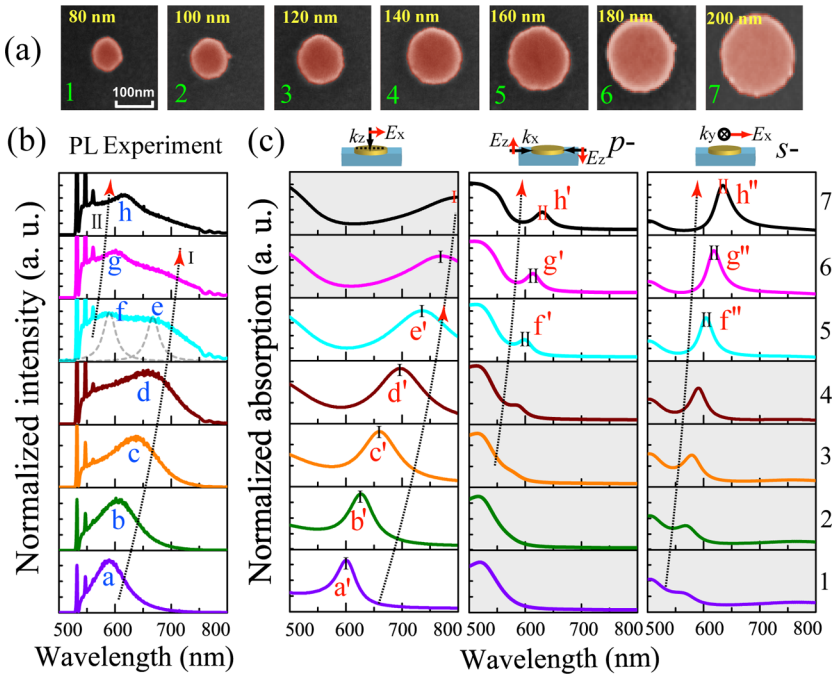

Figure 1. (a) Scanning electron microscope (SEM) images of gold nanodisks with diameters ranging from 80 to 200 nm. (b) Experimental PL spectra (excitation wavelength of 532 nm) of different gold nanodisks. The dashed gray curves are obtained from the ideal Lorenz curve fitting results. In PL measurements, the polarization direction for both excitation and collection is along the *x* direction. The numerical aperture of the objective lens is 0.95. (c) Simulated absorption spectra of different gold nanodisks when the vertical and horizontal components of plane-wave vectors are considered. By comparing the resonant peaks that are mapped onto the PL spectra, we denote the white and gray areas as contributed and noncontributed areas, respectively. The vertical excitation dominates the contribution when *D* is smaller than 160 nm; 180 is a coupling size where both vertical and horizontal excitations make contributions. After 180 nm, the horizontal excitation dominates the contribution.

although plasmon-mediated PL in gold nanoparticles and nanostructures is being intensively studied,[22−28] investigations on the fundamental spectral response of plasmon-mediated PL in gold nanostructures, with individual sizes beyond the quasi-static limit (∼100 nm),[29,30] are still lacking, where the retardation effects under oblique incidence conditions would become more pronounced.[31,32] Since the retardation effects excited by the horizontal wave-vector component could bring additional plasmonic resonant states that are essentially different from LSPR, it remains an open topic of whether plasmon-mediated PL emission can also originate from these retardation-based plasmonic channels.

In this paper, we present a systematic investigation on the PL spectra in individual and coupled gold nanodisks, with increasing size from below to beyond the quasi-static limit (80−200 nm). It is shown that under oblique incidence two series of red-shifted peaks are observed in the PL of gold nanodisks with increasing size. These peaks are due to the contribution of plasmonic states, which satisfies LSPR or retardation-based cavity-resonant conditions in the absorption spectra for vertical and horizontal wave-vector components, respectively. The experimental evidence indicates that the plasmon-mediated PL emission can be preferentially excited and probed in certain directions and polarizations due to the different plasmonic resonant states available. We also propose a three-step model to well describe the contribution of vertical and horizontal plasmonic resonant states in plasmon-mediated PL.

We first discuss the probing of vertical and horizontal plasmonic resonant states in the PL spectra of individual gold nanodisks. Figure 1a shows the scanning electron microscope (SEM) images of individual gold nanodisks, which have a diameter from 80 to 200 nm. The gold nanodisks with a thickness of 30 nm were fabricated on SiO_2/Si substrates through electron-beam lithography (EBL) and lift-off processes (see Methods). Figure 1b presents the measured PL spectra of these gold nanodisks under an excitation wavelength of 532 nm. The numerical aperture (NA) of the objective lens used in the measurement is 0.95 (100× magnification), i.e., an incident angle of about 71.8°. At this oblique incidence condition, the gold nanodisks were illuminated by both vertical and horizontal wave-vector components.

As shown in Figure 1b, there are two series of monotonically red-shifted peaks, i.e., "Peak I", when *D* is increased from 80 nm to 160 nm, and "Peak II", when *D* varies from 160 to 200 nm. These two series of peaks can also be confirmed from the measured dark-field scattering spectra, as shown in Figure S1a. We find that "Peak I" and "Peak II" are preferentially excited by vertical and horizontal wave-vector components, respectively. The critical size for transition from vertical-wave-vector-contributed to horizontal-wave-vector-contributed peaks is about 160 nm. This conclusion is well supported by the simulated absorption spectra for separated vertical and horizontal wave-vectors, as shown in Figure 1c, where the contributed and noncontributed areas are denoted as white and gray areas, respectively. First, from the absorption spectra for vertical wave-vector k_z (with electric field E_x), there exists only a monotonic red-shifted main series of peaks (denoted as I) when *D* is increased from 80 nm to 200 nm. As a result, the peaks a−e in the PL spectra are attributed to the absorption peaks a′−e′. Second, from the absorption spectra for two horizontal plane-wave vectors k_x (p-polarization with out-of-plane electric field E_z) and k_y (s-polarization with in-plane electric field E_x), we observe a monotonically red-shifted series

DOI: 10.1021/acsphotonics.5b00308
ACS Photonics 2015, 2, 1217−1223

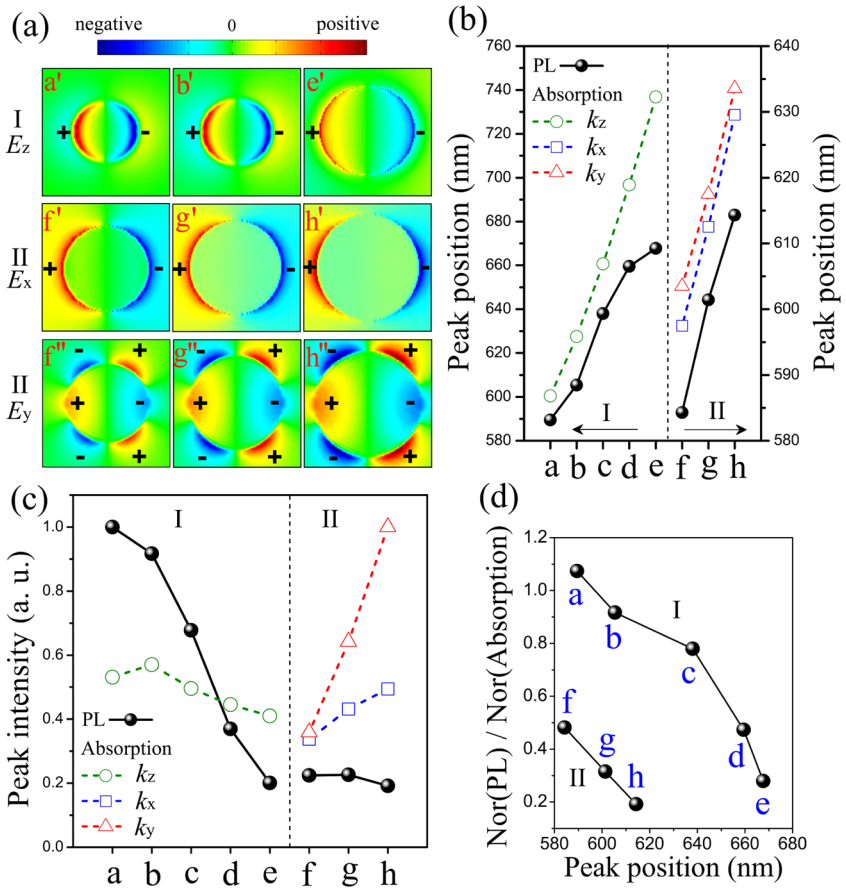

Figure 2. (a) Near-field amplitude distribution (in the $x-y$ plane) of respective electric-field components for the selected peaks in Figure 1c. The electric-field component along the incident wave-vector direction can be used to denote the charge distribution. (b, c) Peak position and intensity of selected peaks in the PL (solid line) and absorption (dashed lines) spectra, respectively. (d) Ratio of normalized PL intensity/normalized absorption intensity at peaks a–g in the PL spectra under an excitation of 532 nm.

of peaks (denoted as II) when D is increased from 160 nm to 200 nm. These peaks f–h in the PL spectra arise predominantly from the excitation by horizontal plane-wave vector k_y with in-plane electric field E_x.

Let us discuss the physical origin of "Peak I" and "Peak II". Figure 2a shows the respective spatial distribution of the electric-field amplitude, i.e., E_x, E_y, and E_z, in the near-field region, from the selected peaks of "Peak I" and "Peak II" in Figure 1c. "Peak I" originated from the dipolar LSPR when the nanodisk is polarized by electric field E_x. According to Gans's extension formulation for solving the Mie-scattering absorption cross section of nanodisks,[33] the resonant wavelength of dipolar LSPR will show a consistent red-shift with an increasing disk diameter.

Interestingly, "Peak II" is observed to be the cavity resonance due to retardation effects, where a short-range surface plasmon polariton (SPP) is propagating along the x or y direction and interfering with the reflected SPP to finally form a standing wave in the gold nanodisks.[32] We can observe clear dipolar charge distributions for peaks f′–h′ and hexapole-like charge distributions for peaks f″–h″. They are the results of retardation-induced charge distributions by out-of-plane electric field E_z and in-plane electric field E_x, respectively. The condition of cavity-resonant SPP (CR-SPP) can be written as[32]

$$\frac{2\pi n_{SPP} D}{\lambda_R} = m\pi - \phi \quad (1)$$

Here, n_{SPP} is the effective refractive index of surface plasmon propagation modes. ϕ is the phase shift acquired upon reflection at the ends of the nanodisk. As a result, the resonant wavelength λ_R will follow the red-shifted rule with increasing diameter of gold nanodisks. For example, at the absorption peak λ_R = 597 nm (f′), n_{SPP} is calculated to be 2.02 according to the effective refractive index formulation.[32] Therefore, assuming ϕ is zero, the first-order (m = 1) CR-SPP should occur at D = 148 nm, which is very close to the actual diameter 160 nm. The real ϕ is calculated as about -0.09π. It is different from the case of a long-range SPP, which shows a reflection phase ϕ of $\sim 0.35\pi$ at the edge of a semi-infinite gold film.[34]

Figure 2b–d present comprehensive comparisons between PL and absorption spectra on the peak position and intensity. First, as compared to absorption peaks, the peak position of the PL peaks (a–h) is always blue-shifted, which is especially prominent for larger gold nanodisks (Figure 2b). Second, the peak intensity of either PL peaks a–e or g and h always gradually decreases with increasing diameter of the gold nanodisks, which is particularly confusing for PL peaks f–h because the corresponding absorption peaks have the opposite behavior (Figure 2c). A similar mismatch between PL spectra and scattering spectra in the peak position and intensity can also be observed in Figure S1c and d.

To better understand these behaviors, we propose here a simple three-step model of the plasmon-mediated PL process for gold nanodisks (see Figure 3):

DOI: 10.1021/acsphotonics.5b00308
ACS Photonics 2015, 2, 1217–1223

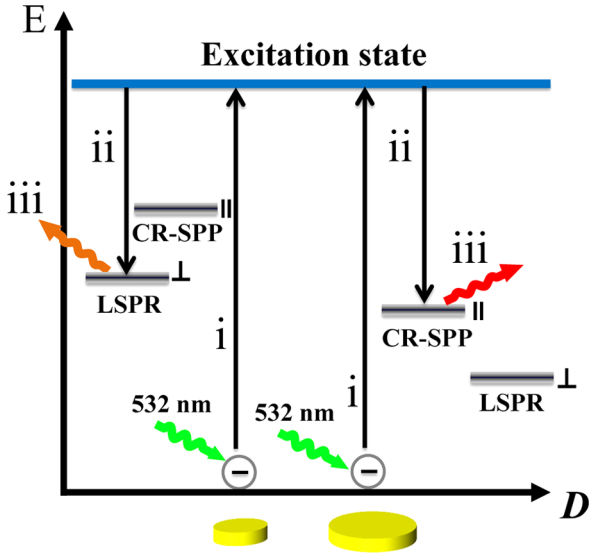

Figure 3. Schematic illustration of three-step model of the plasmon-mediated PL process for gold nanodisks. Electrons are driven from the energy ground state to the excitation state, then undergo nonradiative relaxation, and finally radiate mainly through LSPR and CR-SPP plasmonic channels, which are excited by vertical and horizontal wave-vector components, respectively. For relatively small and larger nanodisks, the LSPR and CR-SPP are preferentially excited at glancing angles, respectively.

(i) Excitation. When using a 532 nm laser, both the d−sp interband transition of bound electrons and the collective oscillation of sp-band free electrons from the ground energy state to a higher-energy state are possible in principle.[6,24,25] These two processes cannot be separated because of their spectral overlap.[25]

(ii) Nonradiative relaxation. Due to electron−electron and electron−phonon interactions, the excited electrons undergo nonradiative relaxation and reach thermal equilibrium.[10,35]

(iii) Radiative emission. The relaxed electrons eventually damp mainly through ultrafast LSPR and CR-SPP plasmonic channels and become radiative emission.[6,7] For relatively small and large nanodisks, the LSPR and CR-SPP are preferentially excited at glancing angles, respectively.

Therefore, the excitation and radiative emission steps in PL of gold nanodisks are strongly modulated by the resonant plasmonic states mapped in the absorption and scattering spectra.[28] The mismatch between PL spectra and absorption/scattering spectra in peak position and intensity is due to the nonradiative relaxation process of photoexcited carriers. This decay process usually follows an exponential profile in time scale.[35] In particular, Figure 2d shows the ratio of normalized peak intensity between PL under excitation of 532 nm and absorption peaks. The intensities of either peaks a−e or peaks f−h contributed are inversely proportional to the peak position. This is direct evidence to imply the influence of nonradiative relaxation of electrons in the PL process.[36]

To give more evidence for the probing of vertical and horizontal plasmonic resonant states, we have also investigated the size-dependent PL spectra of two coupled circular gold nanodisks with a specific gap, i.e., the gold nanodisk dimer. This model is different from previous works on gold dimers, which were focused on the gap-dependent optical responses.[36−38] In particular, the gap of dimers in our model is fixed to be 30 nm to guarantee a relatively strong coupling between two gold nanodisks. Figure 4a shows the SEM images of different gold

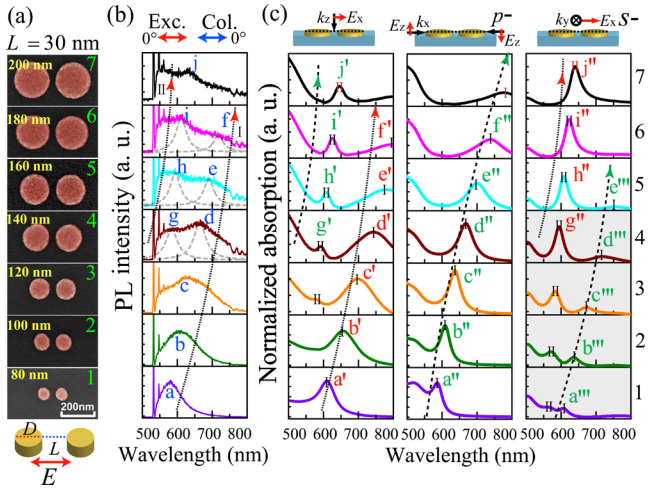

Figure 4. (a) SEM images of two coupled gold nanodisks with diameters ranging from 80 to 200 nm and a fixed gap of 30 nm. (b) Experimental PL spectra (excitation wavelength of 532 nm) of different gold dimers. The dashed gray curves are obtained from the ideal Lorenz curve fitting results. In PL, both excitation and collection are along the interparticle axis (longitudinal polarization, 0°−0°). The numerical aperture of the objective lens is 0.95. (c) Simulated absorption spectra of different gold dimers when the vertical and horizontal components of plane-wave vectors are considered. The white and gray areas denote contributed and noncontributed areas, respectively. The contribution area is more complex than that for single nanodisks. In the conjunction area of the dimer, the vertical excitation always makes a contribution to the high-order peaks. On the boundary of the dimer, the horizontal excitation of k_x always dominates the contribution of fundamental peaks.

nanodisk dimers when the diameter of individual nanodisks varies from 80 to 200 nm. The measured PL spectra (under excitation−collection 0°−0°) of these gold nanodisk dimers are shown in Figure 4b. The corresponding dark-field scattering spectra are shown in Figure S1b.

In general, the PL spectra for gold nanodisk dimers are quite similar to those for individual gold nanodisks, except the following two aspects: (i) The main series of "Peak I" is more prominent for those relatively large gold nanodisk dimers (see peaks d−f). (ii) The critical diameter of the gold nanodisk for the observation of the clear main series of "Peak II" is advanced to 140 nm.

In fact, the contribution of vertical and horizontal plasmonic resonant states is more complicated for gold nanodisk dimers. Figure 4c shows the simulated absorption spectra of gold nanodisk dimers, which present some different absorption properties as compared to individual gold nanodisks. The higher-order peaks (dashed line) are now observed even in the case of normal incidence, which was absent in the single disks. Similarly, the fundamental mode (denoted as I) can be seen for the horizontal incidence. Lastly, the original higher-order mode that is due to CR-SPP is absent in the wave-vector excitation along x.

Figure 5a shows the electric-field component distribution of selected peaks of fundamental and higher-order modes in Figure 4c. For the case of the vertical wave-vector, the additional higher-order mode results from the quadrupole−

DOI: 10.1021/acsphotonics.5b00308
ACS Photonics 2015, 2, 1217−1223

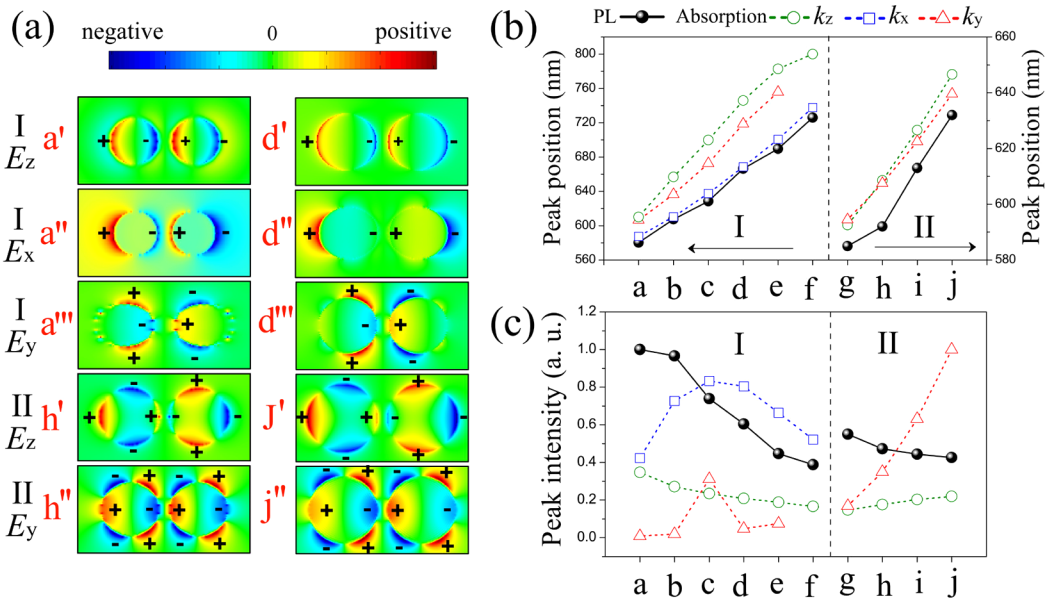

Figure 5. (a) Spatial distribution of electric-field amplitude in the near-field region (in the $x-y$ plane) of the selected peaks of the simulated absorption spectra for different gold dimers from Figure 4c. (b, c) Peak position and intensity of selected peaks in PL and absorption spectra of different gold dimers, respectively.

quadrupole bonding of LSPR (see h′ and j′). For the case of the horizontal wave-vector k_x, the additional fundamental mode looks like dipole−dipole bonding and it is actually due to the retardation effect of the LSPR peak when the SPP propagates along the interparticle axis of the gold nanodisk dimers.

Figure 5b and c give further comparisons on the peak position and intensity of main peaks in PL and absorption spectra. Similar to individual gold nanodisks, the peak position of PL peaks is always blue-shifted and the peak intensity of the PL peaks will gradually decrease with increasing size of the gold nanodisk dimers. One important sign is that the intensity of the absorption peaks for k_z is always lower than that for k_x or k_y. This implies that in the final PL spectra the horizontal plasmonic states play a critical role.

Lastly, we also investigated the influence of using the excitation laser with a higher energy of 2.71 eV (i.e., 457 nm) or using a smaller NA of the objective lens (NA = 0.45) on the PL of individual gold nanodisks. When a 457 nm laser was used (Figure S2), besides the expected vertical and horizontal plasmonic resonant peaks, an additional series of peaks, which are due to the bulk absorption of the gold film, can be observed. When a smaller NA was used (Figure S3), a slight degeneration of "Peak II" can be observed due to the decreased excitation of horizontal plasmonic resonant states. Furthermore, to support the partially depolarized behavior in the PL process, the PL for gold nanodisk dimers when the excitation−collection angles are 0°−90° was also measured, as shown in Figure S4.

In conclusion, for both individual and coupled gold nanodisks, we have successfully probed two series of red-shifted peaks with increasing diameter of gold nanodisks from 80 to 200 nm. These peaks are essentially due to the LSPR and CR-SPP, which are plasmonic resonant states preferentially excited by the vertical and horizontal wave-vector components, respectively. The mismatch between PL and absorption spectra in peak position and peak intensity is due to the influence of nonradiative relaxation of photoexcited carriers during the PL progress. It is expected that the more interesting and complex retardation-based plasmonic resonant states can be preferentially excited and probed at glancing angles in the PL of other complex or asymmetric gold nanostructures with sizes beyond the quasi-static limit.

METHODS

Electron-Beam Lithography. The gold nanodisk samples were patterned on SiO_2/Si substrates using electron-beam lithography. PMMA resist (950 K molecular weight, 1.67% in anisole) from MicroChem Corp. was spin-coated at 3k rpm to be ∼80 nm on SiO_2/Si substrates. The thickness of SiO_2 was 100 nm. We chose silicon as the substrate so as to avoid charging effects during the EBL process, while 100 nm SiO_2 was used as a spacer layer to avoid the reduction of plasmon damping caused by the silicon substrate. After spin coating, the substrates were baked on a hot plate at 180 °C for 120 s. EBL was done with an Elionix ELS-7000 system with an accelerating voltage of 100 keV and a beam current of 100 pA. An optimized exposure dose was used to obtain the structures we designed for the measurements. After exposure, the samples were developed with 1:3 MIBK/IPA developer at low temperature (−10 °C) for 15 s and then directly blown dry with a steady stream of N_2. Low-temperature development of PMMA provides higher contrast and pattern resolution. Metal deposition was performed using an electron-beam evaporator (Explorer Coating System, Denton Vacuum). A 30 nm thick gold layer was deposited with a 1 nm thick Cr adhesion layer. The working pressure during the evaporation was $<5 \times 10^{-7}$ Torr. The temperature of the sample chamber was kept at 20 °C during the entire evaporation process, with the sample holder rotating at a rate of 50 rpm to ensure the uniformity of deposition. Lift-off was done by immersing samples in *N*-methylpyrrolidone (NMP) solvent at an elevated temperature of 65 °C.

Optical Measurements. For the gold nanodisk samples, the PL and dark-field scattering spectra[36,39] were measured on a confocal Raman microscopy system (WITec CRM200). The spectra were dispersed by a 150 lines/mm grating and detected using a TE-cooled CCD (Andor DV 401-BV-351). A high-

DOI: 10.1021/acsphotonics.5b00308
ACS Photonics 2015, 2, 1217−1223

resolution spectrograph (0.55 nm/pixel) allows peak positions of spectra to be measured accurately within ±1 nm. The integration time was set as 20 s, and a piezoelectric stage was used to approach the maximum luminescence intensity.

Numerical Simulations. All simulated absorption spectra of gold nanostructures were completed on the software platform FDTD Solutions (Lumerical Solutions, Inc.) based upon the three-dimensional finite difference time-domain (FDTD) method. The structural parameters of gold nanostructures for modeling were set according to the size measured from SEM images. The complex dielectric constants for gold, SiO_2, and Si were from Johnson-Christy and Palik, respectively. The mesh accuracy was set as 6, and an extrafine mesh with a size of 1 nm in the $x-y$ plane and 2 nm along the z direction was added around the gold nanostructures. A perfectly matched layer (PML) boundary condition was set for all three dimensions.

■ ASSOCIATED CONTENT

Supporting Information

(S1) Dark-field scattering spectra of individual and coupled gold nanodisks. (S2) PL of individual gold nanodisks when a higher-energy excitation laser (457 nm) was used. (S3) PL of individual gold nanodisks when a smaller NA = 0.45 objective lens was used. (S4) PL of gold nanodisk dimers when the excitation−collection angles are 0°−90°. The Supporting Information is available free of charge on the ACS Publications website at DOI: 10.1021/acsphotonics.5b00308.

■ AUTHOR INFORMATION

Corresponding Authors

*E-mail: joel_yang@sutd.edu.sg (J. K. W. Yang).
*E-mail: zexiang@ntu.edu.sg (Z.-X. Shen).

Author Contributions

#L. Jiang and T. Yin contributed equally to this work.

Notes

The authors declare no competing financial interest.

■ ACKNOWLEDGMENTS

This work was supported by Singapore Ministry of Education Academic Research Fund Tier 2 (Grant No. MOE2012-T2-2-124) and Tier 3 (Grant No. MOE2011-T3-1-005), the Natural Science Foundation of China (No. 61205042), and the Natural Science Foundation of Jiangsu Province in China (No. BK20141393). L.Y.J. also would like to acknowledge the financial support from the Zijin Intelligent Program of NUST (No. 2013_zj_010203_16). Z.G.D., S.J.T., X.M.G., and J.K.W.Y. would like to acknowledge the funding support from the Agency for Science, Technology and Research (A*STAR) Young Investigatorship (Grant No. 0926030138), SERC (Grant No. 092154099), and National Research Foundation (Grant No. NRF-CRP 8-2011-07).

■ REFERENCES

(1) Mooradian, A. Photoluminescence of metals. *Phys. Rev. Lett.* **1969**, *22*, 185−187.
(2) Boyd, G. T.; Yu, Z. H.; Shen, Y. R. Photoinduced luminescence from the noble-metals and its enhancement on roughened surfaces. *Phys. Rev. B: Condens. Matter Mater. Phys.* **1986**, *33*, 7923−7936.
(3) Link, S.; El-Sayed, M. A. Shape and size dependence of radiative, non-radiative and photothermal properties of gold nanocrystals. *Int. Rev. Phys. Chem.* **2000**, *19*, 409−453.
(4) Mohamed, M. B.; Volkov, V.; Link, S.; El-Sayed, M. A. The 'lightning' gold nanorods: fluorescence enhancement of over a million compared to the gold metal. *Chem. Phys. Lett.* **2000**, *317*, 517−523.
(5) Huang, T.; Murray, R. W. Luminescence of tiopronin monolayer-protected silver clusters changes to that of gold clusters upon galvanic core metal exchange. *J. Phys. Chem. B* **2003**, *107*, 7434−7440.
(6) Beversluis, M. R.; Bouhelier, A.; Novotny, L. Continuum generation from single gold nanostructures through near-field mediated intraband transitions. *Phys. Rev. B: Condens. Matter Mater. Phys.* **2003**, *68*, 115433.
(7) Dulkeith, E.; Niedereichholz, T.; Klar, T. A.; Feldmann, J.; von Plessen, G.; Gittins, D. I.; Mayya, K. S.; Caruso, F. Plasmon emission in photoexcited gold nanoparticles. *Phys. Rev. B: Condens. Matter Mater. Phys.* **2004**, *70*, 205424.
(8) Bouhelier, A.; Bachelot, R.; Lerondel, G.; Kostcheev, S.; Royer, P.; Wiederrecht, G. P. Surface plasmon characteristics of tunable photoluminescence in single gold nanorods. *Phys. Rev. Lett.* **2005**, *95*, 267405.
(9) Farrer, R. A.; Butterfield, F. L.; Chen, V. W.; Fourkas, J. T. Highly efficient multiphoton-absorption-induced luminescence from gold nanoparticles. *Nano Lett.* **2005**, *5*, 1139−1142.
(10) Varnavski, O. P.; Goodson, T.; Mohamed, M. B.; El-Sayed, M. A. Femtosecond excitation dynamics in gold nanospheres and nanorods. *Phys. Rev. B: Condens. Matter Mater. Phys.* **2005**, *72*, 235405.
(11) Zheng, J.; Zhou, C.; Yu, M. X.; Liu, J. B. Different sized luminescent gold nanoparticles. *Nanoscale* **2012**, *4*, 4073−4083.
(12) Bourret, G. R.; Ozel, T.; Blaber, M.; Shade, C. M.; Schatz, G. C.; Mirkin, C. A. Long-range plasmophore rulers. *Nano Lett.* **2013**, *13*, 2270−2275.
(13) Choo, H.; Kim, M. K.; Staffaroni, M.; Seok, T. J.; Bokor, J.; Cabrini, S.; Schuck, P. J.; Wu, M. C.; Yablonovitch, E. Nanofocusing in a metal-insulator-metal gap plasmon waveguide with a three-dimensional linear taper. *Nat. Photonics* **2012**, *6*, 837−843.
(14) Viarbitskaya, S.; Teulle, A.; Marty, R.; Sharma, J.; Girard, C.; Arbouet, A.; Dujardin, E. Tailoring and imaging the plasmonic local density of states in crystalline nanoprisms. *Nat. Mater.* **2013**, *12*, 426−432.
(15) Jager, S.; Kern, A. M.; Hentschel, M.; Jager, R.; Braun, K.; Zhang, D.; Giessen, H.; Meixner, A. J. Au nanotip as luminescent near-field probe. *Nano Lett.* **2013**, *13*, 3566−3570.
(16) Greybush, N. J.; Saboktakin, M.; Ye, X. C.; Della Giovampaola, C.; Oh, S. J.; Berry, N. E.; Engheta, N.; Murray, C. B.; Kagan, C. R. Plasmon-enhanced upconversion luminescence in single nanophosphor-nanorod heterodimers formed through template-assisted self-assembly. *ACS Nano* **2014**, *8*, 9482−9491.
(17) Lee, J.; Hernandez, P.; Govorov, A. O.; Kotov, N. A. Exciton-plasmon interactions inmolecular spring assemblies of nanowires and wavelength-based protein detection. *Nat. Mater.* **2007**, *6*, 291−295.
(18) Wu, X.; Ming, T.; Wang, X.; Wang, P. N.; Wang, J. F.; Chen, J. Y. High-photoluminescence-yield gold nanocubes: for cell imaging and photothermal therapy. *ACS Nano* **2010**, *4*, 113−120.
(19) Mertens, H.; Koenderink, A. F.; Polman, A. Plasmon-enhanced luminescence near noble-metal nanospheres: Comparison of exact theory and an improved Gersten and Nitzan model. *Phys. Rev. B: Condens. Matter Mater. Phys.* **2007**, *76*, 115123.
(20) Shahbazyan, T. V. Theory of plasmon-enhanced metal photoluminescence. *Nano Lett.* **2013**, *13*, 194−198.
(21) Titus, E. J.; Willets, K. A. Accuracy of superlocalization imaging using gaussian and dipole emission point-spread functions for modeling gold nanorod luminescence. *ACS Nano* **2013**, *7*, 6258−6267.
(22) Yorulmaz, M.; Khatua, S.; Zijlstra, P.; Gaiduk, A.; Orrit, M. Luminescence quantum yield of single gold nanorods. *Nano Lett.* **2012**, *12*, 4385−4391.
(23) Fang, Y.; Chang, W. S.; Willingham, B.; Swanglap, P.; Dominguez-Medina, S.; Link, S. Plasmon emission quantum yield of single gold nanorods as a function of aspect ratio. *ACS Nano* **2012**, *6*, 7177−7184.
(24) Lumdee, C.; Yun, B. F.; Kik, P. G. Gap-plasmon enhanced gold nanoparticle photoluminescence. *ACS Photonics* **2014**, *1*, 1224−1230.

DOI: 10.1021/acsphotonics.5b00308
ACS Photonics 2015, 2, 1217−1223

(25) Zhang, T. Y.; Lu, G. W.; Shen, H. M.; Shi, K. B.; Jiang, Y. Y.; Xu, D. S.; Gong, Q. H. Photoluminescence of a single complex plasmonic nanoparticle. *Sci. Rep.* **2014**, *4*, 3867.
(26) Verellen, N.; Denkova, D.; De Clercq, B.; Silhanek, A. V.; Ameloot, M.; Van Dorpe, P.; Moshchalkov, V. V. Two-photon luminescence of gold nanorods mediated by higher order plasmon modes. *ACS Photonics* **2015**, *2*, 410−416.
(27) Andersen, S. K. H.; Pors, A.; Bozhevolnyi, S. I. Gold photoluminescence wavelength and polarization engineering. *ACS Photonics* **2015**, *2*, 432−438.
(28) Guan, Z. P.; Gao, N. Y.; Jiang, X. F.; Yuan, P. Y.; Han, F.; Xu, Q. H. Huge enhancement in two-photon photoluminescence of Au nanoparticle clusters revealed by single-particle spectroscopy. *J. Am. Chem. Soc.* **2013**, *135*, 7272−7277.
(29) Kelly, K. L.; Coronado, E.; Zhao, L. L.; Schatz, G. C. The optical properties of metal nanoparticles: The influence of size, shape, and dielectric environment. *J. Phys. Chem. B* **2003**, *107*, 668−677.
(30) Tam, F.; Chen, A. L.; Kundu, J.; Wang, H.; Halas, N. J. Mesoscopic nanoshells: Geometry-dependent plasmon resonances beyond the quasistatic limit. *J. Chem. Phys.* **2007**, *127*, 204703.
(31) Kottmann, J. P.; Martin, O. J. F. Retardation-induced plasmon resonances in coupled nanoparticles. *Opt. Lett.* **2001**, *26*, 1096−1098.
(32) Sondergaard, T.; Bozhevolnyi, S. Slow-plasmon resonant nanostructures: Scattering and field enhancements. *Phys. Rev. B: Condens. Matter Mater. Phys.* **2007**, *75*, 073402.
(33) Gans, R. The state of ultramicroscopic silver particles. *Ann. Phys.* **1915**, *352*, 270−U14.
(34) Zhu, D.; Dong, Z. G.; Chu, H. S.; Akimov, Y. A.; Yang, J. K. W. Image dipole method for the beaming of plasmons from point sources. *ACS Photonics* **2014**, *1*, 1307−1312.
(35) Voisin, C.; Christofilos, D.; Loukakos, P. A.; Del Fatti, N.; Vallee, F.; Lerme, J.; Gaudry, M.; Cottancin, E.; Pellarin, M.; Broyer, M. Ultrafast electron-electron scattering and energy exchanges in noble-metal nanoparticles. *Phys. Rev. B: Condens. Matter Mater. Phys.* **2004**, *69*, 195416.
(36) Hu, H. L.; Duan, H. G.; Yang, J. K. W.; Shen, Z. X. Plasmon-modulated photoluminescence of individual gold nanostructures. *ACS Nano* **2012**, *6*, 10147−10155.
(37) Wissert, M. D.; Ilin, K. S.; Siegel, M.; Lemmer, U.; Eisler, H. J. Coupled nanoantenna plasmon resonance spectra from two-photon laser excitation. *Nano Lett.* **2010**, *10*, 4161−4165.
(38) Huang, W. Y.; Qian, W.; Jain, P. K.; El-Sayed, M. A. The effect of plasmon field on the coherent lattice phonon oscillation in electron-beam fabricated gold nanoparticle pairs. *Nano Lett.* **2007**, *7*, 3227−3234.
(39) Lei, D. Y.; Fernandez-Dominguez, A. I.; Sonnefraud, Y.; Appavoo, K.; Haglund, R. F.; Pendry, J. B.; Maier, S. A. Revealing plasmonic gap modes in particle-on-film systems using dark-field spectroscopy. *ACS Nano* **2012**, *6*, 1380−1386.

DOI: 10.1021/acsphotonics.5b00308
ACS Photonics 2015, 2, 1217−1223